# 2D materials-assisted heterogeneous integration of semiconductor membranes toward functional devices •

Cite as: J. Appl. Phys. **132**, 190902 (2022); https://doi.org/10.1063/5.0122768 Submitted: 25 August 2022 • Accepted: 25 October 2022 • Published Online: 16 November 2022

Minseong Park, 🗓 Byungjoon Bae, Taegeon Kim, et al.

## **COLLECTIONS**

EP ·

This paper was selected as an Editor's Pick







# ARTICLES YOU MAY BE INTERESTED IN

Two-dimensional material templates for van der Waals epitaxy, remote epitaxy, and intercalation growth

Applied Physics Reviews 9, 031305 (2022); https://doi.org/10.1063/5.0090373

Temperature-dependent photoluminescence properties of water-soluble  $CuInS_2$  and  $CuInS_2$ /ZnS quantum dots

Journal of Applied Physics 132, 194306 (2022); https://doi.org/10.1063/5.0105290

Atomic layer-by-layer etching of graphene directly grown on SrTiO<sub>3</sub> substrates for high-yield remote epitaxy and lift-off

APL Materials 10, 041105 (2022); https://doi.org/10.1063/5.0087890

Journal of Applied Physics Special Topics Open for Submissions



# 2D materials-assisted heterogeneous integration of semiconductor membranes toward functional devices

Cite as: J. Appl. Phys. 132, 190902 (2022); doi: 10.1063/5.0122768 Submitted: 25 August 2022 · Accepted: 25 October 2022 · Published Online: 16 November 2022







Minseong Park, Byungjoon Bae, Daegeon Kim, Hyun S. Kum, and Kyusang Lee (1,3,a)





- Department of Electrical and Computer Engineering, University of Virginia, Charlottesville, Virginia 22904, USA
- <sup>2</sup>Department of Electrical and Electronic Engineering, Yonsei University, Seoul 03722, South Korea
- <sup>3</sup>Department of Material Science and Engineering, University of Virginia, Charlottesville, Virginia 22904, USA

#### **ABSTRACT**

Heterogeneous integration techniques allow the coupling of highly lattice-mismatched solid-state membranes, including semiconductors, oxides, and two-dimensional materials, to synergistically fuse the functionalities. The formation of heterostructures generally requires two processes: the combination of crystalline growth and a non-destructive lift-off/transfer process enables the formation of high-quality heterostructures. Although direct atomic interaction between the substrate and the target membrane ensures high-quality growth, the strong atomic bonds at the substrate/epitaxial film interface hinder the non-destructive separation of the target membrane from the substrate. Alternatively, a 2D material-coated compound semiconductor substrate can transfer the weakened (but still effective) surface potential field of the surface through the 2D material, allowing both high-quality epitaxial growth and non-destructive lift-off of the grown film. This Perspective reviews 2D/3D heterogeneous integration techniques, along with applications of III-V compound semiconductors and oxides. The advanced heterogeneous integration methods offer an effective method to produce various freestanding membranes for stackable heterostructures with unique functionalities that can be applied to novel electrical, optoelectronic, neuromorphic, and bioelectronic systems.

Published under an exclusive license by AIP Publishing. https://doi.org/10.1063/5.0122768

#### I. INTRODUCTION

Epitaxy is a universal thin-film growth technique to produce high-quality single-crystalline films<sup>1-4</sup> The epitaxial growth method generally requires lattice-matched (or nearly matched) material systems to carry out high-quality growth with minimal defects. To realize such a growth for modern solid-state electronic and photonic applications, various epitaxial deposition techniques have been developed, such as molecular beam epitaxy (MBE),5 metalorganic chemical vapor deposition (MOCVD),6 pulsed laser deposition (PLD), sputtering, etc.

Using epitaxial growth techniques, heteroepitaxy to form the heterostructure has been developed via consecutive epitaxial growth by adopting lattice-matched and/or lattice-mismatched material systems.<sup>9,10</sup> In addition to conventional monolithic growth techniques, it is also possible to form artificial heterostructures by stacking the thin epitaxial films individually. However, the release

of epitaxially grown thin films from the substrate to create membranes (freestanding forms of thin films) is inevitably destructive since the interfaces of the film and the substrate are strongly bonded to each other. To overcome this issue, various nondestructive lift-off techniques have been developed for the fabrication of freestanding membranes. The fabricated membranes can be heterogeneously integrated onto an arbitrary substrate or stacked with other functional membranes, providing hybrid functionalities of various material systems, including III-V compound semiconductors, silicon, high-k dielectrics, ferroelectrics, magnetics, perovskites, etc. 11-14 Alternatively, wafer etching techniques allow the creation of freestanding membranes by etching the entire bulk substrate. However, non-silicon wafers are generally costly, and the chemical wet etching process can damage the epitaxial film during the long etching time of the bulk wafer.4

One promising non-destructive method to create epitaxial freestanding membranes and hetero-integrated materials systems is

<sup>&</sup>lt;sup>a)</sup>Authors to whom correspondence should be addressed: hkum@yonsei.ac.kr and kl6ut@virginia.edu

2D material-assisted epitaxial growth and transfer techniques. 11 2D materials are atomically thin crystalline solids without surface dangling bonds that atomically connect them with foreign materials, so the relatively weak van der Waals (vdW) force is a major source of the interlayer bonding. Since the 2D interlayer prevents atomic bonding between the substrate and epitaxial films, it allows for the non-destructive separation of the epitaxial films from the substrate while allowing "remote" seeding of the crystallographic structure of the substrate to the epitaxial film. 15 This 2D material-assisted layer transfer (2DLT) technique employs a metal stressor layer deposited on top of the remote epitaxial films to mechanically exfoliate the epitaxial film off of a graphene-coated substrate. 16 By simple stacking, the exfoliated freestanding membrane can then be heterogeneously integrated with other membranes of different crystal structures or materials. Since epitaxial growth generally necessitates a high growth temperature, 6 this ex situ heterogeneous integration is free from thermal budget limitations as well, achieving high compatibility and transferability to host substrates.

This Perspective provides an overview of recent progress in theory, growth, transfer, experimental studies, devices, and the outlook of 2D/3D heterostructure devices based on the 2DLT technique. We first summarize the advances in epitaxy techniques in Sec. II, followed by state-of-the-art lift-off and transfer techniques in Sec. III. We then analyze the 2D/3D heterogeneous integration in Sec. IV and its applications and devices in Sec. V. Sections VI and VII provide the scientific and technological challenges and future directions of 2D material-assisted heterogeneous integration, respectively.

# II. ADVANCES IN EPITAXY TECHNIQUES

The advancement in 2D material-assisted epitaxy technologies opens a new pathway to produce high-quality and high-yield single-crystalline membranes. The recent advancement stems from the 2D interlayers that relax the atomic interaction between the epilayer and the substrate, allowing guided exfoliation at the 2D interlayer/substrate interface. Nevertheless, the fundamental growth of both the target film and the 2D material still relies on conventional epitaxy technologies. In other words, both conventional and advanced technologies complement each other, allowing novel epitaxy and lift-off concepts to be realized. In this section, conventional epitaxy technologies will be introduced first to understand the following advanced technologies, and two advanced epitaxy technologies involving 2D materials will be discussed.

## A. Conventional epitaxy techniques

Conventional epitaxy techniques were developed for either homoepitaxy or heteroepitaxial growth. As shown in Fig. 1(a), homoepitaxy is the epitaxial growth of films that are identical to the underlying substrate. Thus, the dislocation density and interfacial defects of the epitaxial film are nearly non-existent, and the highest quality epilayers can be grown. Various flux sources can be employed for epitaxial growth, such as molecular beam, metalorganic/hydride precursors, and ablated flux for MBE, MOCVD, and PLD, respectively. However, there are three drawbacks to homoepitaxy. First, it is difficult to separate the epitaxial layer off from the parent substrate since there is no obvious atomic

boundary between the substrate and the epilayer. Second, there is only a very limited choice of substrate materials for lattice-matched growth. Third, most advanced electrical and photonic devices require heterojunctions with varying compositions, so homoepitaxy has limited use application wise.

Heteroepitaxy is the growth of epitaxial layers with dissimilar materials compared to the substrate. 18 As shown in Fig. 1(b), due to the differences in the lattice constant, the epitaxial layer is formed on top of the substrate with strain, which depends on the magnitude of the lattice constant difference. If the epitaxial layer is grown very thin, then the epilayer conforms to the in-plane lattice of the substrate (pseudomorphic growth), deformed in the out-of-plane direction from its original relaxed state. If the epitaxial layer is grown beyond a critical thickness, then the built-up strain is released in the form of crystallographic defects such as dislocations. 19 Therefore, the material combination between the substrate and the epitaxial film is still limited, although much more relaxed than homoepitaxy. One commonly used approach to solve this challenge is to employ a buffer layer between the substrate and the target epilayer. The strain induced by the mismatch is confined to the atomic structure of the buffer layer above a certain critical thickness, ranging from a few nanometers to micrometers, depending on the material system. 20,21 Thus, the strain and defects are concentrated in the buffer layer, and reasonably high-quality target epitaxial layers can be grown on top of the strain-relaxed buffer layer that is lattice matched to the active epitaxial layer. One example of the employment of a buffer layer is growing an AlGaN-based buffer on a Si substrate before GaN growth.<sup>22</sup> The large lattice mismatch between GaN and Si can be overcome by the AlGaN-based buffer layer, but there are trade-offs in using buffer layers, such as deteriorated uniformity due to the additional layer and costs associated with growing a thick buffer layer.

# B. 2D-material-assisted epitaxy techniques

2D-material-assisted epitaxy techniques can be categorized as vdW epitaxy (vdWE) and remote epitaxy. 15 Unlike conventional epitaxial growth techniques, 2D-material-based epitaxy techniques feature reliable detachability of the epitaxial layer since 2D materials possess no dangling bonds that can hybridize the atomic orbitals at the heterostructure interface [Fig. 1(c)]. Therefore, the out-of-plane interaction due to the dangling bonds is theoretically non-existent, thereby relaxing the epitaxial strain at the interface. The vdWE was first demonstrated in the mid-1980s, <sup>23</sup> employing a sub-nanometer ultrathin interlayer regarded as a 2D material today. By doing so, the lattice mismatch issue is alleviated to a degree, still enabling the epitaxial growth of the target films. The relaxed strain broadens the permissible range of the lattice and thermal expansion coefficients; for example, vdWE with more than 60% lattice mismatch has been successfully achieved. 15 One main drawback of the vdWE is the absence of the dangling bonds of the 2D materials, which results in the poor wettability of the 2D substrate.2

Remote epitaxy is the other 2D-material-assisted epitaxial technique that employs only a few layers or monolayer of 2D materials so that the substrate surface potential penetrates the thin 2D material, but simultaneously the vdW bonding between the

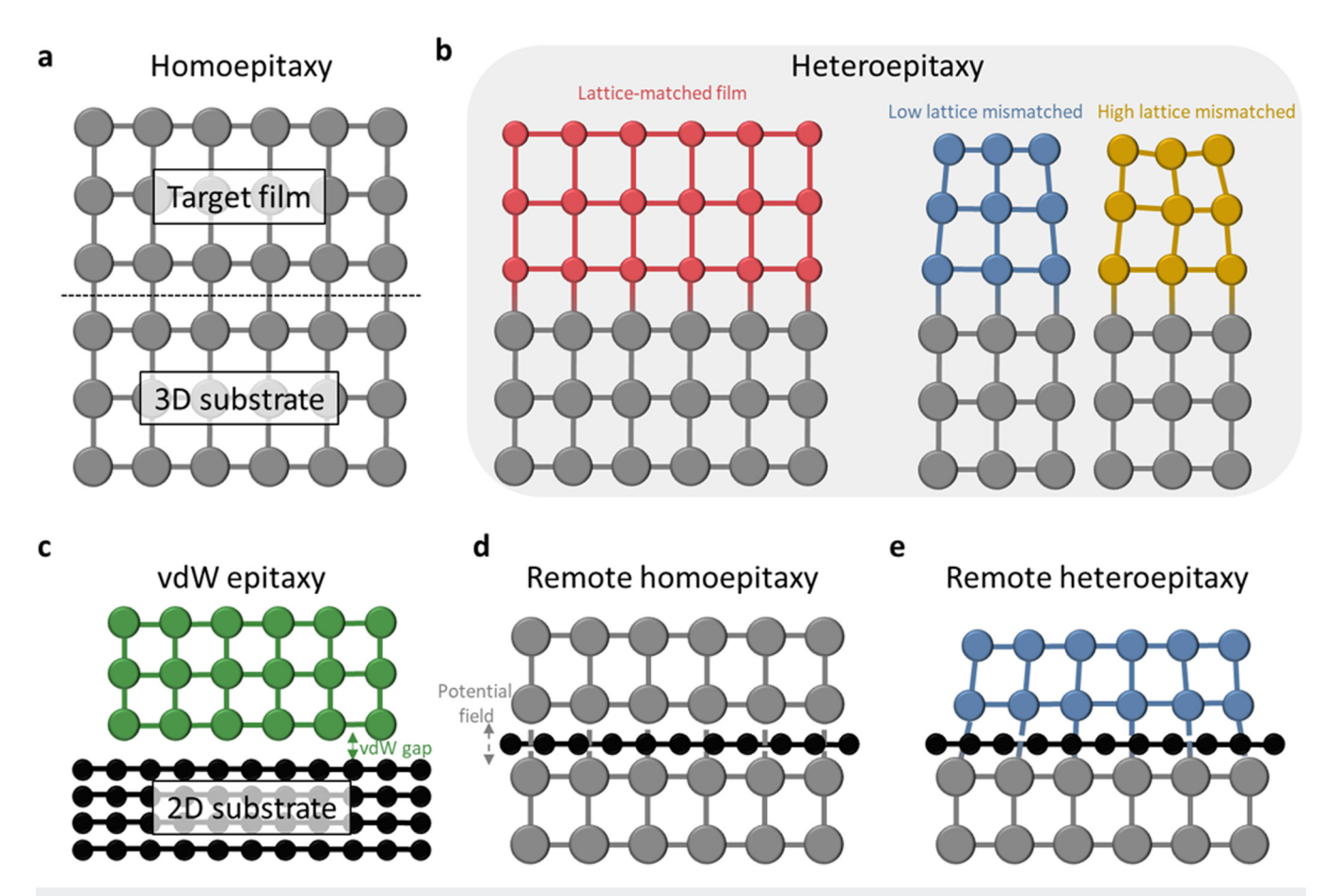


FIG. 1. Schematic illustration of mixed dimensional interfaces under various epitaxy techniques. (a) Lattice-matched homoepitaxy without 2D materials. (b) Heteroepitaxy without 2D materials for lattice-matched (left) and lattice-mismatched (right) heterostructures. (c) Lattice-mismatched van der Waals epitaxy (vdWE) with 2D materials. The vdW gap ensures the high transferability of the target membrane. (d) Lattice-matched remote homoepitaxy incorporating 2D materials. (e) Lattice-mismatched remote heteroepitaxy.

substrate and the epilayer results in improved detachability of the epilayer for freestanding membrane creation [Figs. 1(d) and 1(e)]. 11 Note that without 2D materials, the interfacial heterostructure is hardly separable due to the strong covalent bond between the substrate and the epilayer. In general, a few layers (1-3 layers) of 2D material allow the potential field penetration as well as maintain the vdW force between the 2D materials and the epilayer. In this case, the vdW force dominates the atomic interaction, resulting in a facile separation of the target layers from the 2D surface. As the number of 2D layers increases, the potential field cannot penetrate the 2D stack, resulting in polycrystalline growth. On the other hand, fewer 2D layers elicit a stronger penetration of the potential field toward the growing surface, leading to a high possibility of single-crystal epitaxial growth. The critical 2D material thickness to reliably grow the epilayer is also determined by the polarities (or ionicity) of both the substrate and the 2D material. Such a polarity effect has recently been reported for various ionic material systems such as GaAs, GaN, and LiF, where the strength of the ionicity

limits the maximum number of allowed 2D layers. <sup>13</sup> In addition to the ionic interactions driven by 3D materials (substrates and target layers), the polarity of 2D materials might also be critical at the 2D/3D heterointerface, promoting nucleation and growth of membranes. For example, a recent study of density functional theory (DFT) calculations for the influence of graphene (non-polar) and hexagonal BN (hBN, polar) reveals that GaN substrate potential fluctuation is attenuated by more than half through 1ML hBN than through 1ML graphene. <sup>13</sup>

# III. LIFT-OFF AND TRANSFER TECHNIQUES

Although single-crystalline thin films can be epitaxially grown, additional lift-off and transfer techniques are imperative to produce freestanding membranes applicable to flexible, wearable, and bioinspired electronics<sup>25–27</sup> First reported in 1978, <sup>28</sup> the lift-off process is a separation method between epitaxially grown layers and substrates as 3D/3D heterostructures, and the transfer process is to

attach the separated layers onto foreign substrates. In general, direct epitaxial growth onto the flexible substrates is challenging due to large lattice mismatches, different crystallinities (typically, polymeric materials are employed as the flexible substrates), and vastly different thermal budgets. Thus, novel lift-off and transfer techniques allow the creation of novel heterostructures, including flexible heterostructures on polymeric or organic materials<sup>29–31</sup> In this section, various lift-off and transfer techniques will be explored, including both conventional and 2D-assisted methods, in conjunction with the two-step aspects of separation and adhesion.

Figure 2 demonstrates several epitaxial lift-off techniques for 3D/3D and 2D/3D heterostructures. To separate the layers from the substrate (or from the 2D-on-substrate), conventional lift-off techniques can be carried out chemically, optically, or mechanically. The chemical lift-off technique uses an additional epitaxial sacrificial layer between the substrate and the target membrane, and the entire stack is immersed in a solution that only etches the sacrificial layer. The freestanding membrane is then transferred onto a foreign substrate. After drying the transferred membrane

(eliminating liquid molecules between the substrate and the transferred membrane), the adhesion is maintained by the vdW force bonding between the foreign substrate and the freestanding membrane, which allows further fabrication processes such as photolithography, etching, drying, and cleaning. The wet process, however, incorporates undesired wrinkles, and the etchant could damage (etch) adjunct materials in addition to the sacrificial layer. Therefore, a reliable wet epitaxial lift-off and transfer technique requires a sacrificial layer with extremely high etching selectivity (by employing an additional etch-stop layer) and reliable handling during the transferring process.

In comparison to chemical lift-off, the laser and mechanical lift-off techniques allow transfer of freestanding membranes without immersing membranes into a chemical solution. <sup>31,33</sup> The laser lift-off technique employs a short-wavelength laser that is absorbed by the separating layer, decomposing the interface between the substrate and the target layer. <sup>24</sup> The mechanical lift-off process incorporates an additional deposition of a stressor layer, which spalls the substrate along with the epitaxial layer.

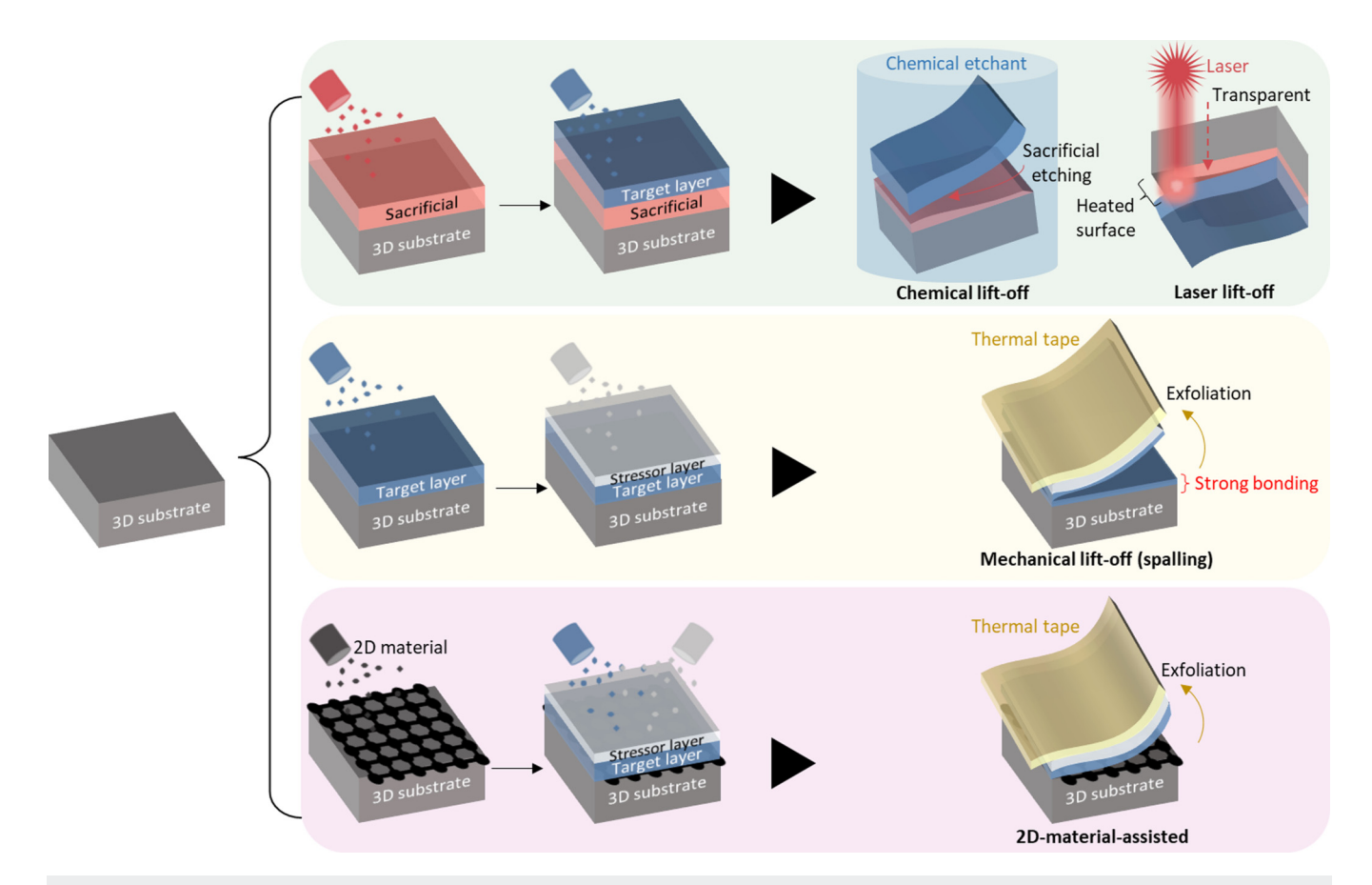


FIG. 2. Schematic illustrations of creation of freestanding membranes. Top row: a sacrificial layer and a target layer can be sequentially deposited onto the substrate. The sacrificial layer is either chemically etched (wet etching process) or optically deformed to lift off the target layer from the substrate. Middle row: an additional Ni stressor is deposited after depositing the target layer onto the substrate. The thermally releasable tape is attached to the Ni stressor surface and destructively exfoliates the target layer from the substrate. Bottom row: the pre-deposited (or pre-transferred) 2D material allows the improved separation of the target layer from the substrate.

The separated membranes with the stressor and tape are then transferred onto foreign substrates. Note that the widely used scotch-tape-based peel-off method is also one of the mechanical lift-off techniques, which allows exfoliation of 2D layers from the bulk material.35,36 Moreover, an adhesive polyimide layer can be spin-coated onto either the epilayer (before the tape is applied to the epilayer) or a foreign substrate, enhancing the transferability of the separated membranes.<sup>37,38</sup> However, mechanical spalling methods are destructive methods since there is no sacrificial layer between the substrate and the epilayer (although not for mechanical exfoliation of two-dimensional vdW materials). This leads to large cracks, thickness variations, and morphological roughness at the separation interface. Furthermore, the applicability of optical lift-off methods is limited since the sacrificial layer needs to be reactive to the optical flux, which might induce high heat and, thus, damage the membranes.

The 2D-material-assisted growth and lift-off techniques can prevent the shortcomings of the abovementioned lift-off techniques. As discussed in Sec. II, the weakened atomic interactions between the interfaces of the epilayer and substrate allow non-destructive separation. The 2DLT technique provides various advantages, including substrate reusability with minimal parent substrate refurbishment and fast and precise layer release from the substrate. Therefore, the 2D-material-assisted heterogeneous integration methods have recently aroused tremendous interest in the semiconductor industry. In Secs. IV–VII, 2D/3D heterostructures for various material systems will be discussed in conjunction with these lift-off and transfer techniques.

# IV. 2D/3D MIXED DIMENSIONAL HETEROGENEOUS INTEGRATION

In this section, we discuss the 2D-assisted epitaxy and transfer techniques for III-V, III-N, and complex-oxides to achieve non-destructive freestanding membranes for heterogeneous integrations.

## A. III-V compound semiconductor membranes

Because of the relaxed lattice matching constraint, vdWE is more effective for heteroepitaxy than conventional epitaxial growth techniques. However, the weak vdW interaction between the substrate and the epilayer can cause insufficient short-range ordering in the epilayer. In addition, vdWE tends to form a rough surface on 3D films grown on 2D substrates. Due to the absence of reactive dangling bonds on the epitaxial surface, the transparency of 2D material to atomic interaction is relatively poor, leading to a Volmer-Weber growth mode and cluster formation.<sup>24</sup> Nucleation layer growth at low temperatures is commonly used to mitigate these effects. 39,40 Also, the wettability for crystalline GaN film growth could be enhanced by depositing a ZnO nanowall buffer layer before the GaN growth on graphene or using a hexagonal boron nitride (hBN) substrate with an AlGaN buffer. The substrates coated with hBN can seed the growth of planar III-N single-crystal films, indicating that the materials can be grown into single-crystals via vdWE.4

The recently investigated remote epitaxy employs one or multiple layers of 2D materials (e.g., graphene, amorphous boron nitride, and hBN) between the epitaxial layer and the substrate. <sup>11</sup> Due to the transparency of the 2D material to the Coulombic interactions

between the atoms and the substrate surface [Figs. 3(a) and 3(b)], the substrate under the graphene plays a crucial role in determining the epitaxial orientation of the grown film. Remote epitaxy suggests that the ionicity of the substrate determines the epitaxial quality of a single-crystal film. Thus, nonionic elemental semiconductors, including Si and Ge, cannot be grown via remote epitaxy. The critical thicknesses of graphene for remote epitaxy of GaAs (30% ionicity), GaN (50% ionicity), and LiF (90% ionicity) are 1, 2, and 3 monolayers, respectively [Fig. 3(c)]. The remote homoepitaxy of GaAs via 1ML graphene shows that the crystalline orientation of grown GaAs is well matched to the parent substrate [Fig. 3(d)]. Also, remote heteroepitaxy was successfully demonstrated for the growth of lattice mismatched InGaP on a GaAs substrate [Fig. 3(e)]<sup>42-</sup> that single-crystalline 3D compound semiconductors can be grown through remote epitaxy (with the optimized number of 2D layers), also implying that the ionicity of the single-crystal substrate is sufficient to transfer the atomic bonding potential to the single-crystal compound film through the graphene layer.

Remote epitaxy is applicable to produce freestanding membranes for heterogeneous integration. Epitaxy films grown through remote epitaxy can be transferred to a foreign substrate via the 2DLT method, in which the host substrate can be flexible, transparent, act as heat sinks, etc. The combination of remote epitaxy and 2DLT alleviates the lattice mismatch restriction that has limited the heterogeneous integration of 3D material-based heterostructures and provides the production cost-reduction of the epitaxial film by allowing reuse of the parent wafer multiple times. 38,47,48

2D/3D heterogeneous integration is dictated by interfacial forces such as ionic-vdW and covalent-vdW. For example, the interfacial coupling mechanism between graphene and ferroelectric materials is by ionic-vdW and covalent-vdW due to the electronegativity difference and crumpling amplitude of graphene at the graphene/ferroelectric interface, respectively. 49 Therefore, a 2D/3D heterogeneous integration system exhibits a more sophisticated coupling effect than vdW interactions among 2D materials and exhibits unique coupling properties (electrical, thermal, etc.)<sup>5</sup> Electrical coupling enables ultrafast charge transfer between weak vdW interfaces at 2D/3D heterojunctions and among 2D materials. The ultrafast charge transfer in atomically thin heterostructures is attributed to the proximity of the two heterostructures (because electrons and holes need to move less than 1 nm vertically for charge transfer). Another essential aspect of electronic devices is thermal management via heat dissipation. AlN or SiC is conventionally used for heat dissipation of light-emitting diodes, power devices, and integrated circuits that generate heat by Joule heating. In contrast, single-layer graphene has a thermal conductivity of  $3000-5000\,\mathrm{Wm}^{-1}\,\mathrm{K}^{-1}$  that is much higher than that of sapphire and SiC (30 and 350 Wm<sup>-1</sup> K<sup>-1</sup>, respectively). As a result, thermal coupling in 3D/2D structures mediates the thermal management significantly, which can improve the device performance without additional energy allocation for heat dissipation.

# B. Complex oxide membranes

Complex-oxide materials feature a wide range of functional properties (piezoelectricity, ferroelectricity, and magneticity) for emerging optoelectronic, spintronic, neuromorphic, and

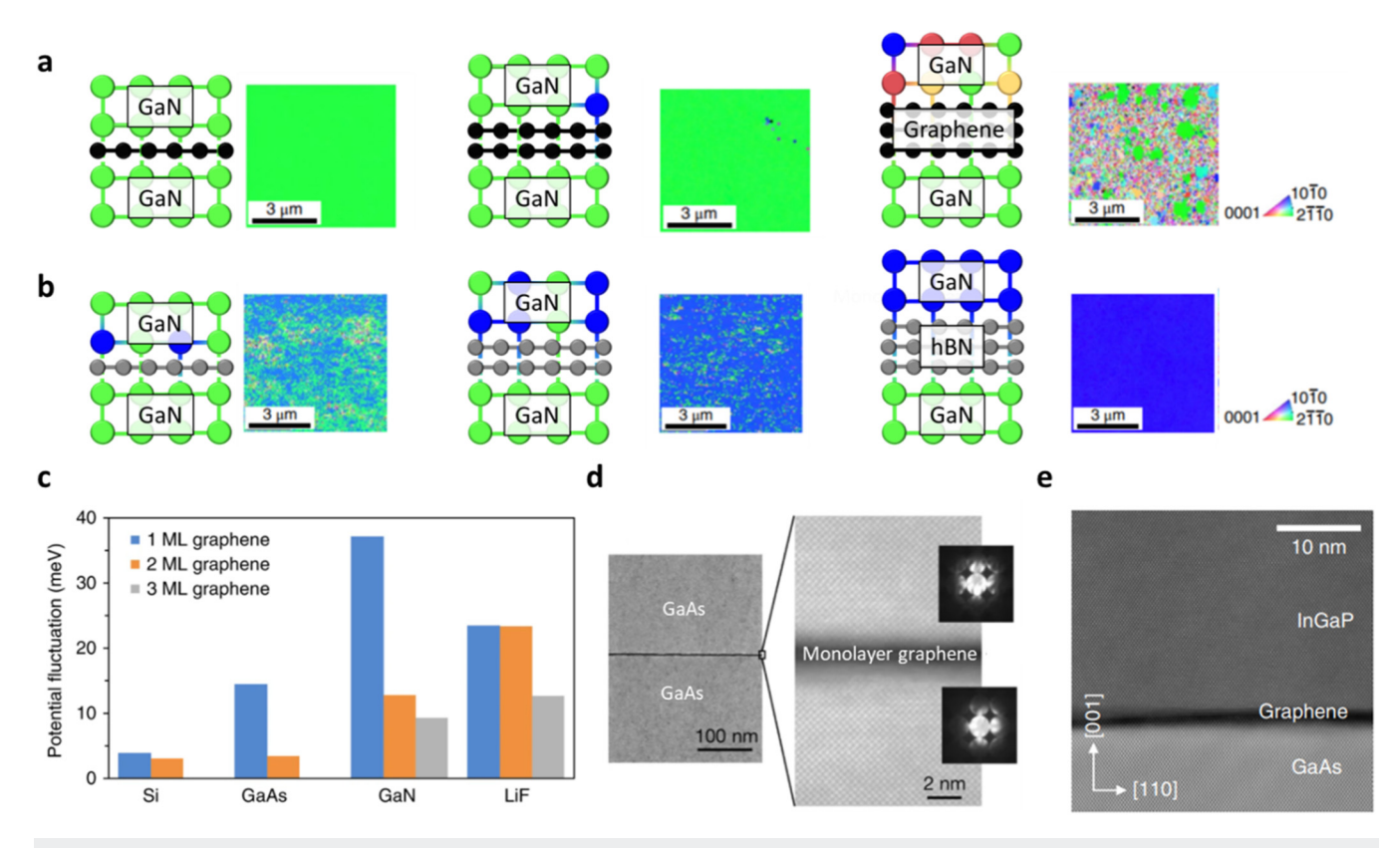


FIG. 3. 2D-material-assisted III–V remote epitaxial growth. Remote homoepitaxy of GaN with various numbers of (a) graphene (black circle) and (b) hexagonal BN (hBN, gray circle) interlayers. The schematic illustration shows the crystallinity of the growing GaN; lime colors exhibit matched crystal orientation, and other colors exhibit mismatched crystal orientation. The electron backscattering diffraction (EBSD) images are correlated to the adjoint schematics. (c) Potential fluctuation for various materials and the number of graphene layers. Reprinted with permission from Kong et al., Nat. Mater. 17, 999–1004 (2018). Copyright 2018 Springer Nature Ltd. (d) Cross-sectional high-resolution scanning transmission electron microscopy (STEM) image of GaAS(001) remote homoepitaxy with 1ML graphene. Convergent-beam electron diffraction patterns from the target layer (top inset) and the substrate (bottom inset). Reprinted with permission from Kim et al., Nature 544, 340–343 (2017). Copyright 2017 Springer Nature Ltd. (e) Cross-sectional annular dark-field STEM (ADF-STEM) image of InGaP/GaAs remote heteroepitaxy with 1ML graphene. Reprinted with permission from Bae et al., Nat. Nanotechnol. 15, 272–276 (2020). Copyright 2020 Springer Nature Ltd.

energy-harvesting devices <sup>13,56-60</sup> These physical functions can be hybridized through heterogeneous integration by stacking multiple layers of such materials. <sup>59,61-64</sup> However, the material combinations and compatibility of complicated oxides are severely limited by lattice mismatch and etch selectivity between the epitaxial layer, sacrificial layer, and seed substrate. <sup>65,66</sup> Note that the strong atomic interaction at the interface governs heteroepitaxy and possibly causes severe degradation or enhancement of the unique physical properties of complex oxides (e.g., piezoelectricity and ferroelectricity). Furthermore, the accommodation of the strain energy leads to a change in the ground state, interdiffusion of a chemical element, and the creation of defects at interfaces. <sup>67</sup>

The bonds between the substrate and the piezoelectric or magnetostrictive epitaxial layer prevent mechanical fluctuations of complex oxides, which is called the substrate clamping effect. <sup>68,69</sup> This effect drastically reduces the piezoelectricity and magnetostriction of the complex-oxide thin film. However, when membranes are in their freestanding form, the substrate clamping effect can be

eliminated<sup>68,70–72</sup> Recently, universal 2DLT methods of producing freestanding single-crystalline membranes have been developed for a wide range of complex-oxide materials, including perovskite, spinel, and garnet crystal structures with varying crystallographic orientations, leading to artificial heterostructures with very high magnetoelectric coupling coefficients. <sup>11,13,14</sup> The magnetoelectric property, correlated to the magnetostrictive and piezoelectric coefficients of constituent components, is dependent on the atomic coupling across the interfaces. <sup>14,73</sup>

Graphene can be used as an interlayer between the substrate and the thin film to reduce the strain and substrate clamping effect. <sup>19</sup> The 2D interlayer reduces atomic interaction, thereby enabling remote epitaxial growth without compromising physical properties [Fig. 4(a)]. The thickness and quality of the interlayer are important for the successful production of a crystalline free-standing oxide membrane. DFT calculation shows that the atomic potential fields from the substrate can penetrate completely through 2ML graphene and partially through 3ML graphene for

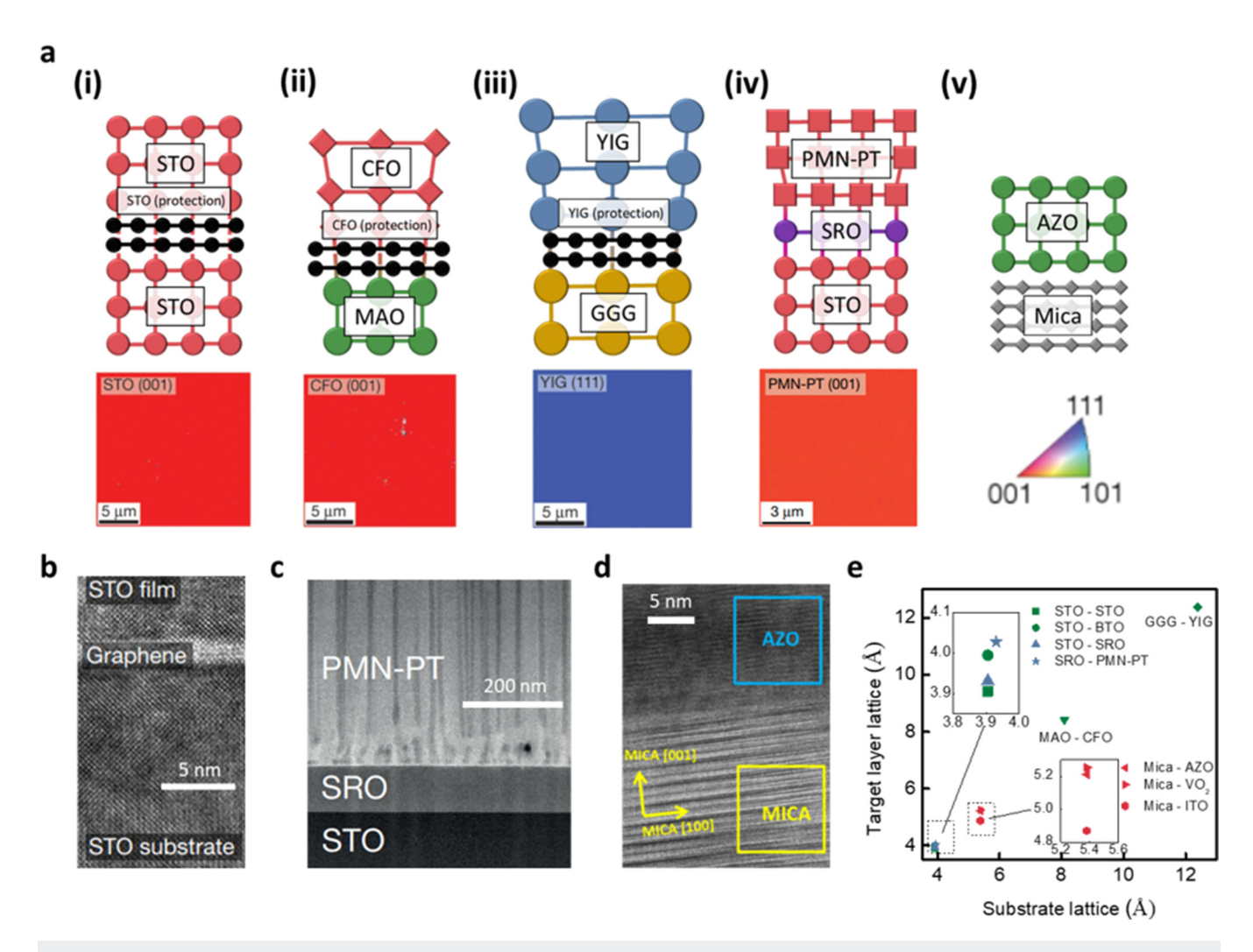


FIG. 4. Epitaxial growth of complex oxide membranes. (a) Various oxide epitaxy including (i) remote homoepitaxy of SrTiO<sub>3</sub> (STO), (ii) remote heteroepitaxy of CoFe<sub>2</sub>O<sub>4</sub> (CFO) onto MgAl<sub>2</sub>O<sub>4</sub> (MAO), (iii) remote heteroepitaxy of garnet Y<sub>3</sub>Fe<sub>5</sub>O<sub>12</sub> (YIG) onto Gd<sub>3</sub>Ga<sub>5</sub>O<sub>12</sub> (GGG), (iv) heteroepitaxy of Pb(Mg<sub>1/3</sub>Nb<sub>2/3</sub>)O<sub>3</sub>-PbTiO<sub>3</sub> (PMN-PT) onto SrRuO<sub>3</sub> (SRO)-coated STO, and (v) vdWE of Al-doped zinc oxide (AZO) onto a mica substrate. Top: schematic illustration of the corresponding epitaxy techniques. Bottom: electron backscattering diffraction (EBSD) images corresponding to each epitaxy schematic. (b) Cross-sectional transmission electron microscopy (TEM) image of STO homoepitaxy with monolayer graphene. (c) High-angle annular dark-field scanning TEM (HAADF STEM) image of PMN-PT heteroepitaxy. Reprinted with permission from Kum *et al.*, Nature 578, 75–81 (2020). Copyright 2020 Springer Nature Ltd. (d) Cross-sectional TEM image of AZO vdWE onto the mica substrate. Reprinted with permission from Bitla *et al.*, ACS Appl. Mater. Interfaces 8, 32401–32407 (2016). Copyright 2016 American Chemical Society. (e) Lattice-dependent heteroepitaxies for oxide membranes.

oxide membranes. <sup>14</sup> In the case of 1ML graphene, the macroscopic holes and tears are easily generated. As a result, the exfoliation yield of the sample with 1ML graphene is comparatively low. Furthermore, the quality of the graphene interlayers is critical for obtaining high-quality and high-yield freestanding crystalline materials, as shown in Fig. 4(b). Note that conventional growth without 2D interlayers also allows for high-quality heteroepitaxy, but freestanding oxide membranes are difficult to obtain due to the strong bonds at the heterointerface [Fig. 4(c)]<sup>74–79</sup> Unlike epitaxy of semiconductor compounds from groups III–V and III-nitrides on graphene, where the substrate and the target material hardly

atomically interact with graphene, avoiding oxidation of graphene during the epitaxy of oxides is crucial to ensure epitaxial release. Any oxidation or damage to the graphene layer prevents successful exfoliation of freestanding crystalline films. Furthermore, organic/metal residues on graphene and non-uniform graphene thickness induce localized polycrystalline growth due to the high sticking coefficient of oxide atoms. It has been reported that the freestanding single-crystal perovskite SrTiO<sub>3</sub> (STO)<sup>82</sup> membrane is obtained by the film exfoliation deposited via PLD, which is grown on a graphene-coated STO (001) substrate. Similarly, single-crystalline CoFe<sub>2</sub>O<sub>4</sub> (CFO)<sup>83</sup> and Y<sub>3</sub>Fe<sub>5</sub>O<sub>12</sub> (YIG)<sup>84</sup> can be grown on

graphene-coated MgAl<sub>2</sub>O<sub>4</sub> (MAO) and Gd<sub>3</sub>Ga<sub>5</sub>O<sub>12</sub> (GGG) substrates by PLD, respectively, followed by the 2DLT technique with a Ni stressor. 14,85 Note that the crystallinity of the freestanding YIG membrane can be improved by the annealing process.86 researchers applied a thin protection layer to avoid the oxidation and etching of the graphene layer in an oxygen environment during deposition, which is effective for all the aforementioned materials.

Compared to ultrathin bare 2D materials that can be damaged in an oxygen environment, bulk 2D layered materials exhibit versatility and compatibility with various processes, which facilitate fabricating freestanding membranes. vdW applied to multilayer 2D materials (e.g., mica) has recently been reported with an abrupt interface, expanding the design possibilities for 2D heteroepitaxy. Note that the substrate under vdWE relaxes stress or strain across the interfaces. Initially, vdWE only referred to the growth of 2D materials on other 2D substrates, but it has since been expanded to include heteroepitaxial growth of 3D materials on 2D substrates. vdW heteroepitaxy on 2D material is an excellent platform for developing oxide heteroepitaxy since it causes no strain or substrate clamping at the interface. Each layer is weakly held together by interlayer cations, resulting in a vdW gap<sup>88-91</sup> One example of 2D materials, muscovite (mica), has a high yield strain, which allows the thickness of a single cleaved sheet to be controlled down to a few micrometers while maintaining superior flexibility.91 epilayer on the mica substrate can be easily peeled off due to the weak vdW interaction, resulting in an unconstrained or freestanding thin film. The 2D structure of the monoclinic mica KAl<sub>2</sub>(AlSi<sub>3</sub>O<sub>10</sub>)(OH)<sub>2</sub> is composed of an AlO<sub>6</sub> octahedral layer sandwiched between two (Si, Al)O<sub>4</sub> tetrahedral layers. Interlayer cations weakly hold these sandwiched layer units with strong covalent bonding inside them, resulting in a vdW gap. Mica is a suitable substrate for vdW heteroepitaxy since cleavage along this vdW gap layer generates two atomically flat surfaces with equal but randomly dispersed K+ cations, sustaining charge neutrality. As a result, the crystalline structure of the mica allows vdWE growth for oxide thin films, resulting in excellent device performance. 92,94,95 Also, mica consists of a well-ordered crystal structure compared to polymer substrates, facilitating epitaxial growth of several inorganic materials such as metal dichalcogenides and oxides. Furthermore, in the ultraviolet-visible-infrared range of the electromagnetic spectrum, a thin mica (100  $\mu$ m) sheet exhibits exceptional transmittance. Furthermore, it is compatible with modern thin film processes due to its high melting point (1150-1300 K), chemical robustness, and compatibility in biomedical and wearable applications. Based on these thermally and chemically stable characteristics, the substrate clamping effect can be alleviated due to the weak vdW force between the mica substrate and the functional films, especially at high temperatures. Therefore, due to the high transparency, atomically clean surface, thermal and chemical stabilities, flexibility, mechanical durability, and compatibility with current production methods, nonmagnetic and insulating mica serve as suitable substrates for flexible optoelectronic applications. As shown in Fig. 4(d), epitaxially grown oxide films on a 2D layered substrate can further facilitate the growth of high-performance planar epitaxial devices that are highly compatible with elevated temperature processes. According to recent studies, mica is an ideal heteroepitaxy substrate for oxide-based flexible and transparent electronics.<sup>97</sup> In this Perspective, various oxide membranes have been grown based on these advanced epitaxy techniques [Fig. 4(e)], and in Sec. V, the corresponding oxide materials and devices will be further discussed.

#### V. APPLICATIONS

The produced freestanding membranes have great advantages in realizing heterogeneous integration due to their freedom from the lattice mismatch constraint. The membranes are applicable to conventional electronic and optical devices by utilizing electrical, optical, and thermal couplings at the heterointerface. The potential applications of the III-V and oxide membranes are discussed in this section.

# A. Applications of heterogeneously integrated compound semiconductor membranes

In this section, the application of 2D materials-assisted heterogeneous integration stemming via vdWE and remote epitaxy will be discussed. Conventional silicon-based semiconductor devices are reaching their development limits in miniaturization, high output power, and high-frequency domains (i.e., Boltzmann tyranny). Accordingly, many researchers are spurring research on next-generation semiconductor devices that can overcome the limitations of silicon. III-V semiconductors exhibit higher mobility and a wider bandgap (more than 2 eV) than Si (1.2 eV). Therefore, III-V semiconductors allow fast switching, high amplification, and superior optoelectronic performance. III-N semiconductors can operate at high temperatures and voltages and feature a critical electric field density 10 times higher than that of Si. In particular, GaN features high electron saturation velocity and a critical electric field; thus, GaN-based devices can significantly increase conduction/switching efficiency and reduce energy loss. 98,99 Therefore, III-N semiconductors are desirable materials in various applications, including high-speed and high-power FETs, radio-frequency electronics, and optoelectronics. We will discuss the wide bandgap semiconductor technologies based on vdWE and remote epitaxy.

Diode: Liu et al. reported the n-MoS<sub>2</sub>/p-GaN rectifying diodes by vdWE. Through Quasi vdWE, a cm-scale uniform MoS<sub>2</sub> film has been grown on a GaN substrate with an ideality factor of up to 1.3 [Fig. 5(a)]. Light-emitting diodes (LEDs) are mainly made of III-V and III-N based compound semiconductors such as GaAs, GaP, GaAsP, and GaN. Recently, a remote epitaxially grown film showed comparable crystalline quality to homoepitaxial GaAs, indicating negligible degradation of material quality during the growth/ transfer process.<sup>11</sup> One example is a flexible GaN PN junction microcrystal-white light emitting diode (MCs-WLED) grown via remote heteroepitaxy. The microrod (MR) PN junction arrays were transferred onto a Cu plate from graphene/c-Al<sub>2</sub>O<sub>3</sub>. The heterogeneously integrated MR LED on the flexible substrate shows a constant electroluminescence during the thousands of bending cycles, providing the path toward the transferrable WLED membrane [Fig. 5(b)]. 100 Another flexible red LED was demonstrated by transferring AlGaInP onto a PET substrate through spalling, exhibiting only a small increase in full width at half maximum (3 nm). Similarly, deep-ultraviolet LEDs (DUV-LEDs) via quasi-vdWE

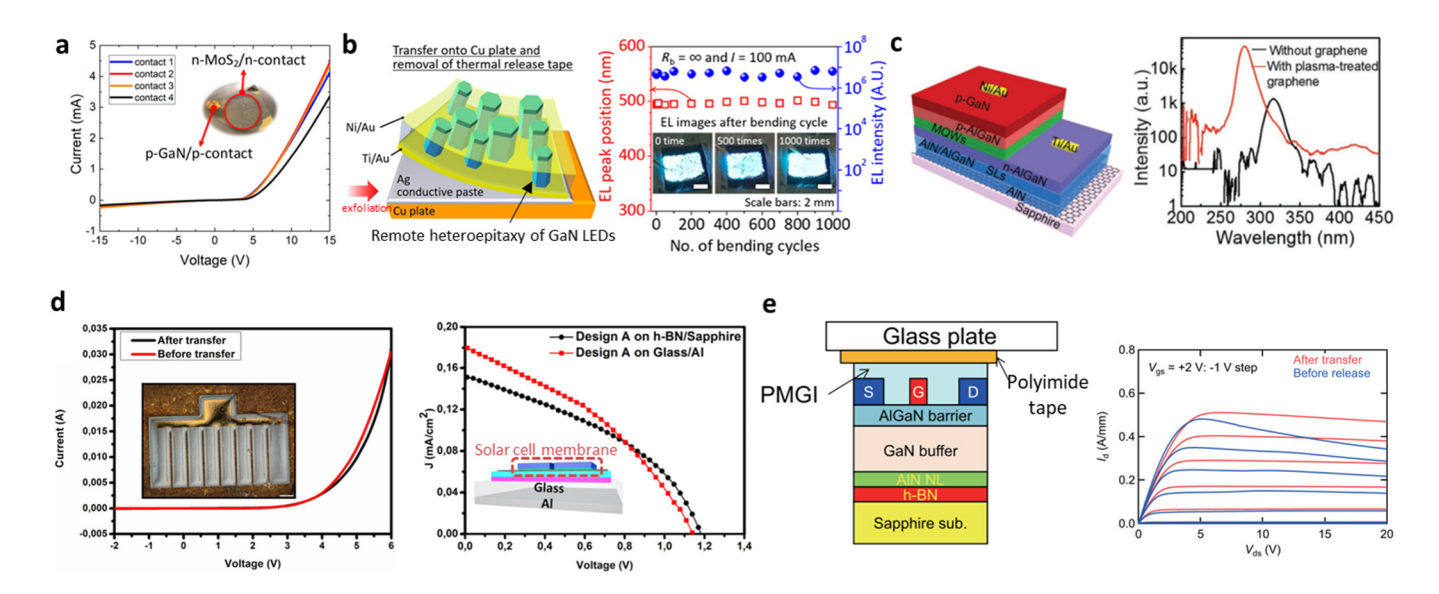


FIG. 5. Applications of heterogeneous integration of III–V films and membranes. (a) Current–voltage (*I*–*V*) characteristics of a monolithically formed n-MoS<sub>2</sub>/p-GaN rectifying diode via vdWE. Reprinted with permission from Liu *et al.*, ACS Appl. Electron. Mater. **2**, 419–425 (2020). Copyright 2020 American Chemical Society. (b) Microrod light-emitting diode (MR LED) membrane from Al<sub>2</sub>O<sub>3</sub> to Cu plate. Left: schematic illustration of the transfer process. Right: electroluminescence (EL) peak position (red empty squares) and intensity (blue soild circles) measured as a function of bending cycle up to 1000 times. Reprinted with permission from Jeong *et al.*, Sci. Adv. **6**, eaaz5180 (2020). Copyright 2020 AAAS. (c) vdWE of AlN for GaN deep-ultraviolet LEDs (DUV-LEDs). Left: schematic illustration of the DUV-LED structure. Right: electroluminescence (EL) spectra of the DUV-LEDs with and without graphene interlayer. Reprinted with permission from Chen *et al.*, Adv. Mater. **31**, 1807345 (2019). Copyright 2019 Wiley. (d) InGaN-based solar cells based on remote heteroepitaxy and freestanding III-N membrane. Left: dark I–V characteristics of the InGaN-based solar cells. Right: current density—voltage (J–V) curves of the InGaN-based solar cells under AM 1.5 illumination condition. Reprinted with permission from Ayari *et al.*, ACS Photonics **5**, 3003–3008 (2018). Copyright 2018 American Chemical Society. (e) AlGaN/GaN high-electron mobility transistor (HEMT) based on vdWE and freestanding III-N membrane. Left: schematic illustration of the transferring process. Right: I<sub>s</sub>–V<sub>ds</sub> characteristics of the AlGaN/GaN HEMT. Reprinted with permission from Hiroki *et al.*, Appl. Phys. Lett. **105**, 193509 (2014). Copyright 2014 AIP Publishing.

have been demonstrated using a plasma-treated graphene that relaxes the strain in the AlN epilayer. The grown graphene interlayer also reduces the dislocation density of the epilayer, exhibiting peak intensity of DUV-LED nearly two orders of magnitude greater than that without graphene [Fig. 5(c)]. 102

Photovoltaic devices: Photovoltaic (PV) cells are optoelectronic devices that convert photons into electricity. The conventional PV cell is based on a diode structure; when the light is illuminated, the photons are absorbed by the active regime of the solar cell, so that holes and electrons are generated in the semiconductor. The PV field focuses on maximizing the power conversion efficiency of photon energy into electrical energy under the constraint of minimal cost. Substrate reusability and flexible solar power generation are possible by epitaxial growth of GaAs on a GaAs and/or Ge substrate, peeling a GaAs thin film through 2DLT, chemical lift-off, mechanical spalling, and transferring it to a flexible substrate. 103 In addition, a simple and inexpensive solar tracking system was implemented by transferring GaAs onto a flexible Kapton substrate via a chemical lift-off technique to form a Kirigami tracking structure. 104 The tilt angle of the Kirigami structure is tunable to track the position of the sun over the course of the day, so yearly energy generation increased between 20% and 40% compared with non-tracking solar systems. Furthermore, an InGaN-based solar cell on an h-BN/sapphire wafer via vdWE has been demonstrated, separated from the

substrate and transferred to a host substrate with a backside reflector.  $^{105}$  This technique increased the short-circuit current density by up to 20% over identical solar cells grown on sapphire [Fig. 5(d)].

High electron mobility transistor: High electron mobility transistor (HEMT) features a large bandgap and high electron mobility in conjunction with the formation of 2D electron gas (2DEG). GaAs-based HEMTs consist of unintentionally doped GaAs, undoped AlGaAs, and undoped GaAs cap layers. AlGaAs features a wider bandgap than that of GaAs, and the Fermi level of the AlGaAs/GaAs heterojunction is higher than the conduction band energy of GaAs where the 2DEG is formed. The HEMT features high current density and fast switching capability for fast-switching FETs, power devices, and RF electronics. However, in heterogeneous structures such as GaN on Si and GaN on SiC, a thick buffer layer is required to alleviate the lattice mismatch constraint, making it difficult to dissipate heat. This can be solved via the vdWE or remote epitaxy techniques. Hiroki et al. reported the fabrication of AlGaN/GaN HEMT on a Cu plate by transferring the active device structure from sapphire [Fig. 5(e)]. Notably, it is expected that excellent heat dissipation can be realized by transferring the HEMT structure to a foreign heat sink (diamond or SiC) via the 2DLT process, which is expected to improve the durability of HEMTs in extreme environments such as ultra-high voltage. 100

# B. Applications of heterogeneously integrated complex oxide films

Many studies have reported the fabrication of freestanding oxide membranes, such as archetypal perovskite STO, perovskite BaTiO<sub>3</sub> (BTO), <sup>108</sup> spinel CFO, and garnet YIG. The remote epitaxy method is applicable to growing these materials to create high-quality freestanding membranes.

Freestanding BTO films and CFO films can be heterogeneously integrated to achieve strain-mediated multi-ferroelectricity. A freestanding BTO-CFO heteroepitaxial nanostructure is able to be epitaxially grown in both out-of-plane and in-plane directions. Because of the highly organized CFO nanopillars embedded in a single crystalline BTO matrix, the heterostructure is free of substrate constraints. As a result, the self-assembled nanostructure is extremely flexible and mechanically sound, capable of spontaneously curling into a tube and being bent with a radius as small as 4.23  $\mu$ m. Furthermore, both microscopic and macroscopic scales of piezoelectricity and ferromagnetism are exhibited, proving its strong multiferroicity at ambient temperature.

 $Pb(Mg_{1/3}Nb_{2/3})O_3\text{-}PbTiO_3$  (PMN-PT) is a freestanding complex oxide composite that can be epitaxially grown by using  $SrRuO_3$  (SRO) as a seed substrate. However, since thin film

PMN-PT is usually deposited by magnetron sputtering (oxygen environment), 110 the graphene-based remote epitaxy is incompatible with the oxide composite. Instead, the SRO substrate can provide a weak interface with PMN-PT, allowing PMN-PT films to be mechanically released without graphene. A Ni stressor deposited on the PMN-PT layer will concentrate the strain at the PMN-PT/ SRO interface and allow atomically precise crack propagation through the interface. Based on the quality and crystallinity of freestanding PMN-PT membranes, robust mechanical coupling with the CFO film was reported with a high transfer yield (>90%). Figure 6(a) shows the stacking of freestanding CFO membranes onto freestanding PMN-PT membranes to create a composite multiferroic. The freestanding CFO/PMN-PT structure is useful for generating a strain-mediated electric field that tailors the magnetism in CFO and generates magnetic field-induced voltage across PMN-PT via fused magnetostriction and piezoelectricity of CFO and PMN-PT, respectively. 111 Another heterogeneous device has also been demonstrated by using an Al-doped zinc oxide (AZO) freestanding film fabricated onto a mica substrate [Fig. 6(b)]. The AZO-Ni-AZO (ANA)/muscovite memristor meets all the most stringent requirements for a transparent soft device, indium tin oxide, including optical transparency of more than 80% in visible

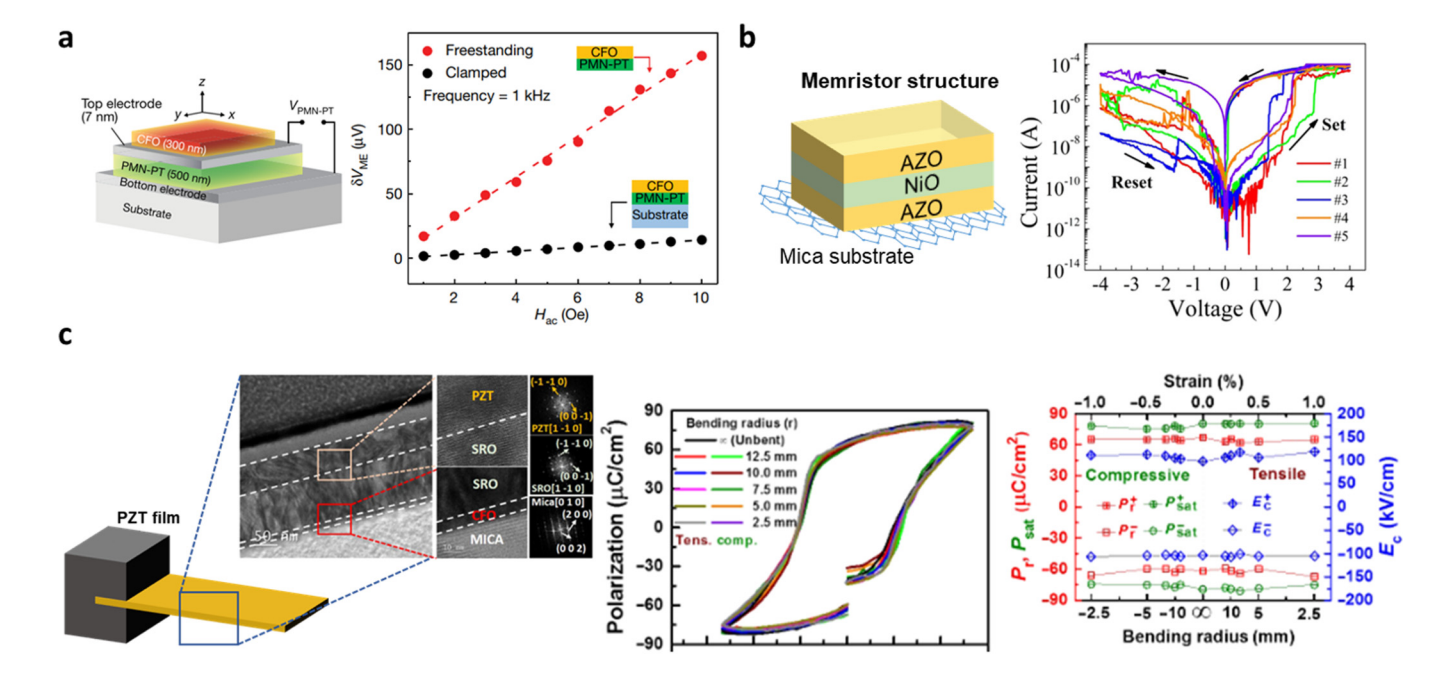


FIG. 6. Applications of heterogeneous integration of complex oxide films and membranes. (a) CFO/PMN-PT magnetoelectric device based on remote heteroepitaxy and vdWE of freestanding CFO and PMN-PT, respectively. Left: schematic illustration of the CFO/PMN-PT device. Right: the voltage induced across the PMN-PT (δV<sub>ME</sub>) as a function of the alternating-current magnetic field strength at a frequency of 1 kHz.<sup>14</sup> Reprinted with permission from Kum *et al.*, Nature 578, 75–81 (2020). Copyright 2020 Springer Nature Ltd. (b) vdWE of the AZO/NiO/AZO memristor. Left: schematic illustration of the AZO/NiO/AZO memristor. Right: *I*-V hysteresis loop of the AZO/NiO/AZO memristor. The printed with permission from Le *et al.*, Nano Energy 56, 322–329 (2019). Copyright 2019 Elsevier. (c) vdWE of a PZT-based flexible ferroelectric device. Left: schematic illustration and cross-sectional TEM image of the device. Middle: polarization–electric field (P–E) hysteresis loops of the device under bending conditions. Right: polarizations and electric field variations as a function of bending radius. (2017) Reprinted with permission from Jiang *et al.*, Sci. Adv. 3, e1700121 (2017). Copyright 2017 AAAS.

light, high performance (ON/OFF resistance ratio >  $10^5$ ), steady endurance to  $10^3$  cycles, and a long retention duration of 105 s. Figure 6(b) describes the I-V curves of the ANA/muscovite heterostructure, which shows the memristive properties.  $^{112}$ 

Furthermore, with a high Curie temperature (793 K) and substantial magnetocrystalline and magnetostrictive anisotropy, CFO possesses outstanding magnetic characteristics. The CFO thin film can be grown on the single-crystalline mica (001) substrate using PLD techniques. The hysteresis loops at various bending conditions show almost identical characteristics, which can be attributed to magnetocrystalline anisotropy. The magnetic characteristics and controllable deformation of the CFO/mica heterostructure emphasize the potential of flexible magnetostrictive films in flexible electronic applications. 114

vdWE with a mica substrate was utilized to epitaxially grow lead zirconium titanate (PZT). Figure 6(c) describes the structure of PZT/SRO/CFO (sacrificial layer)/mica. These single-crystalline flexible ferroelectric PZT films not only maintain decent performance, reliability, and thermal stability comparable to their rigid counterparts but also show remarkable mechanical properties with robust operation in bent states (bending radii down to 2.5 mm) and repetitive tests (1000 times).

#### VI. CHALLENGES

Maintaining pristine interfaces via ultraclean transfer or direct growth procedures is critical for forming 3D/2D heterostructures. Therefore, a reliable procedure must be devised for the creation of large-scale and high-quality graphene. However, the poor scalability of laboratory fabrication processes and a lack of well-defined control parameters for the growth kinetics of 2D materials have hindered the widespread application of 2D materials-based heterointegration. One alternative is to circumvent the 2D layer transferring process by establishing monolithic growth of both graphene and the epitaxial layer. To achieve monolithic graphene formation, a suitable carbon source is required, one that allows the carbon precursor to decompose at low temperatures. Methane is generally used as the carbon precursor for CVD-grown graphene on a copper substrate, which is cracked at a substrate temperature above 800 °C. In contrast, the group V elements (As and P) are extremely volatile in compound semiconductors and desorb at relatively low temperatures (As and P for 600 and 500 °C, respectively). 115,116 As a result, it is suggested that a suitable precursor be chosen for the decomposition at low temperatures when growing the graphene. For example, liquid carbon sources such as toluene are a potential candidate for low temperature (600 °C) growth of monolayer graphene.1

Moreover, surface contaminants generated by adhesive polymers on the substrate limit the seamless remote epitaxial contact due to the sensitivity of remote epitaxy to the interaction gap between the substrate and the epilayer. In addition, metal nanoparticles may remain during the 2DLT process, potentially reducing the device reliability and accelerating the device degradation due to metal particle migration (causing leakage paths or shorting). 117 It is preferable to investigate a new transfer method without harnessing metals or adhesive polymers for fully integrating 2D materials into commercial optoelectronic and electrical devices.

In the case of wafer-scale exfoliation and growth methods using 2D materials, it is important to monitor the nanoscale defects and impurities such as tears, holes, and wrinkles in 2D materials. In particular, the handling of graphene interlayers causes tears in the layer, obstructing remote epitaxial growth and causing partial destructive exfoliation. Due to these difficulties, more research is needed into fabrication of large-scale monolayer graphene on compound semiconductors that are free of physical imperfections while reducing the contact gap between the graphene and the substrate. In addition, a thorough understanding of device performance affected by defects in 2D materials needs to be studied. New or existing methods can be used to enable fast and robust detection of defects; confocal laser scanning has recently been reported as a non-destructive method for probing macroscopic defects in graphene films with a fast turnaround time.

In this Perspective, the 3D/2D structure has mainly been discussed, but the other 2D/3D mixed-dimensional structure has also been investigated 119-121 However, unlike the 3D/2D structure, the 2D/3D structure has three main challenges: (1) precise thickness control during the growth, (2) the limited number of growable 2D materials, and (3) non-destructive transfer process. Recent studies have shown that it is possible to precisely control a few 2D materials such as MoS<sub>2</sub>, <sup>122</sup> MoTe<sub>2</sub>, <sup>123</sup> and graphene, <sup>124</sup> but the thickness controllability extremely depends on the ubiquitous environment, including temperature, humidity, pressure, and chamber geometry. Further investigation into optimizing the growth conditions is required. Additionally, unlike general bulk 3D materials, the 2D materials feature an atomically layered structure; thus, the number of growable 2D materials is limited.<sup>125</sup> The transfer process of the 2D membrane is also challenging since the 2D interface is easily contaminated during the transfer process. In this regard, freestanding production via the 2D/3D structure is still challenging; the destructive scotch-tape method is currently employed for smallscale device fabrication.11

## VII. OUTLOOK

Heterogeneous integration is achieved by epitaxial growth on 2D materials and lift-off transfer techniques, offering improved transferability compared to destructive transfer techniques. In particular, the 2D interlayers between the substrate and the target membrane are held by van der Waals force with a minimal gap that allows penetration of electrostatic potential from the underlying substrate; thus, both epitaxial growth and transferability are achieved. We also discussed the ionicity effect of the 2D material for graphene and hBN 2D materials, suggesting that the ionicity of the 2D material plays a key role in tuning both pristine epitaxial growth and transferability. In this regard, other major 2D counterparts are also potentially applicable to remote epitaxy and vdWE with their different polarities, such as transition metal dichalcogenides (TMDs), 126 black phosphorous (BP), 127 and ferroelectric 2D materials (e.g., In<sub>2</sub>Se<sub>3</sub>, SnS, SnTe, and CuInP<sub>2</sub>S<sub>6</sub>). <sup>128</sup> The electrical coupling properties of the various 2D materials and external electrical fields could modulate the doping concentration of the 2D material and even the target membrane as well. Therefore, such 2D-assisted advanced epitaxy techniques can boost the versatility of 2D electronics in conjunction with the 2D/3D artificial

heterostructures. To date, several electrical and optical devices have been implemented via remote epitaxy and vdWE, such as LEDs<sup>100,129</sup> and PDs.<sup>130,131</sup> Based on these functional devices, 2D-assisted epitaxy techniques are without a doubt universally applicable to other tiers of devices such as HEMTs and RF filters, while they can also be stacked on CMOS circuitry.

In the case of the oxide membranes, the unwanted substrate clamping effect can be eliminated via weak vdW interaction of 2D interlayers or 2D substrates. General epitaxy techniques for the oxides are discussed: remote homoepitaxy, remote heteroepitaxy, and vdWE. The remote epitaxy for the oxide membranes has been optimized via 2ML graphene with an ultrathin protection oxide layer to protect the 2D interlayers from oxygen-based plasma deposition techniques such as sputtering and ALD. <sup>14</sup> Alternatively, the restricted nucleation of the target oxide could be improved via surface treatments, ALD process modifications, and the utilization of freestanding oxide membranes. <sup>132</sup>

Moreover, the production of both freestanding compound semiconductors and oxide membranes has great advantages in terms of low-cost, lattice-mismatch-free, and electrical/optical/ thermal couplings among artificial heterostructures. The artificial heterostructures exhibit tunable energy bands at the heterointerfaces, which can provide unprecedented couplings of electrons, photons, and phonons. The stacked freestanding membranes, thus, feature synergistic functionalities and realize third-order nanocircuitry from each layer and heterointerface without external bulk metal interconnections, 133 resulting in minimized parasitic capacitance and inductance that delay and temporally attenuate the propagating signals. 134 The production of freestanding membranes also guarantees heterogeneous integration of the films onto foreign substrates such as glass and flexible platforms. 135,13 materials-assisted heterogeneous integration will offer an alternative pathway toward interconnection-free multifunctional nanocircuitry for deployable fields such as bioelectronics, optoelectronics, neuromorphic computing, and electromagnetic engineering.

# **ACKNOWLEDGMENTS**

This work was supported by the National Science Foundation (NSF) (Grant No. NSF ECCS-1942868) and U.S. Department of Energy Office of Energy Efficiency and Renewable Energy (EERE) under the Solar Energy Technologies Office (Grant No. DE-EE0008588). The team from Yonsei University would like to acknowledge support from the National Research Foundation of Korea (NRF) (Grant No. 2022M3D1A208522811).

#### **AUTHOR DECLARATIONS**

#### **Conflict of Interest**

The authors declare no conflict of interest.

#### **Author Contributions**

Minseong Park: Conceptualization (equal); Data curation (equal); Formal analysis (lead); Investigation (equal); Project administration (equal); Resources (equal); Visualization (equal); Writing – original draft (lead); Writing – review & editing (equal). Byungjoon Bae: Data curation (equal); Formal analysis (equal); Investigation

(equal); Resources (equal); Visualization (equal); Writing – original draft (equal); Writing – review & editing (equal). **Taegeon Kim:** Data curation (supporting); Formal analysis (supporting); Resources (supporting); Writing – original draft (supporting); Writing – review & editing (supporting). **Hyun S. Kum:** Supervision (equal); Validation (equal); Writing – review & editing (equal). **Kyusang Lee:** Conceptualization (equal); Funding acquisition (equal); Supervision (equal); Validation (equal); Writing – review & editing (equal).

#### **DATA AVAILABILITY**

The data that support the findings of this study are available from the corresponding authors upon reasonable request.

#### **REFERENCES**

<sup>1</sup>K. Lee, J. D. Zimmerman, T. W. Hughes, and S. R. Forrest, Adv. Funct. Mater. 24, 4284 (2014).

<sup>2</sup>D. Fan, K. Lee, and S. R. Forrest, ACS Photonics 3, 670 (2016).

<sup>3</sup>C.-W. Cheng, K.-T. Shiu, N. Li, S.-J. Han, L. Shi, and D. K. Sadana, Nat. Commun. 4(1), 1577 (2013).

<sup>4</sup>L. Shen, L. Wu, Q. Sheng, C. Ma, Y. Zhang, L. Lu, J. Ma, J. Ma, J. Bian, and Y. Yang, Adv. Mater. **29**(33), 1702411 (2017).

<sup>5</sup>B. A. Joyce, Rep. Prog. Phys. 48, 1637 (1985).

<sup>6</sup>L. Sun, G. Yuan, L. Gao, J. Yang, M. Chhowalla, M. H. Gharahcheshmeh, K. K. Gleason, Y. S. Choi, B. H. Hong, and Z. Liu, Nat. Rev. Methods Primers 1, 5 (2021).

<sup>7</sup>R. Kumar, G. Kumar, and A. Umar, J. Nanosci. Nanotechnol. 14, 1911 (2014).
<sup>8</sup>H. S. Lee, Y. Baek, Q. Lin, J. Minsu Chen, M. Park, D. Lee, S. Kim, and K. Lee, Adv. Intell. Syst. 3, 2000202 (2020).

<sup>9</sup>A.-L. Barabasi, Appl. Phys. Lett. **70**, 2565 (1997).

<sup>10</sup>P. Falcaro, K. Okada, T. Hara, K. Ikigaki, Y. Tokudome, A. W. Thornton, A. J. Hill, T. Williams, C. Doonan, and M. Takahashi, Nat. Mater. 16(3), 342–348 (2017).

<sup>11</sup>Y. Kim, S. S. Cruz, K. Lee, B. O. Alawode, C. Choi, Y. Song, J. M. Johnson, C. Heidelberger, W. Kong, S. Choi, K. Qiao, I. Almansouri, E. A. Fitzgerald, J. Kong, A. M. Kolpak, J. Hwang, and J. Kim, Nature 544, 340 (2017).

<sup>12</sup>J. Moon, W. Ma, J. H. Shin, F. Cai, C. Du, S. H. Lee, and W. D. Lu, Nat. Electron. 2, 480 (2019).

<sup>13</sup>W. Kong, H. Li, K. Qiao, Y. Kim, K. Lee, Y. Nie, D. Lee, T. Osadchy, R. J. Molnar, D. K. Gaskill, R. L. Myers-Ward, K. M. Daniels, Y. Zhang, S. Sundram, Y. Yu, S. Bae, S. Rajan, Y. Shao-Horn, K. Cho, A. Ougazzaden, J. C. Grossman, and J. Kim, Nat. Mater. 17, 999 (2018).

<sup>14</sup>H. S. Kum, H. Lee, S. Kim, S. Lindemann, W. Kong, K. Qiao, P. Chen, J. Irwin, J. H. Lee, and S. Xie, Nature 578(7793), 75–81 (2020).

<sup>15</sup>H. Kum, D. Lee, W. Kong, H. Kim, Y. Park, Y. Kim, Y. Baek, S.-H. Bae, K. Lee, and J. Kim, Nat. Electron. 2, 439 (2019).

16Y. Lee, H. H. Tan, C. Jagadish, and S. K. Karuturi, ACS Appl. Electron. Mater. 3(1), 145–162 (2020).

<sup>12</sup>A. N. Khodan, S. Guyard, J.-P. Contour, D.-G. Crété, E. Jacquet, and K. Bouzehouane, Thin Solid Films 515, 6422 (2007).

<sup>18</sup>K. Ludwiczak, A. K. Dabrowska, J. Binder, M. Tokarczyk, J. Iwański, B. Kurowska, J. Turczyński, G. Kowalski, R. Bożek, and R. Stępniewski, ACS Appl. Mater. Interfaces 13, 47904 (2021).

<sup>19</sup>S.-H. Bae, K. Lu, Y. Han, S. Kim, K. Qiao, C. Choi, Y. Nie, H. Kim, H. S. Kum, and P. Chen, Nat. Nanotechnol. 15(4), 272–276 (2020).

<sup>20</sup>H. Lu, W. J. Schaff, J. Hwang, H. Wu, G. Koley, and L. F. Eastman, Appl. Phys. Lett. **79**, 1489 (2001).

<sup>21</sup>S. Çörekçi, M. K. Öztürk, A. Bengi, M. Çakmak, S. Özçelik, and E. Özbay, J. Mater. Sci. 46, 1606 (2011).

- <sup>22</sup>K. J. Chen, O. Häberlen, A. Lidow, C. L. Tsai, T. Ueda, Y. Uemoto, and Y. Wu, IEEE Trans. Electron Devices **64**, 779 (2017).
- <sup>23</sup> A. Koma, K. Sunouchi, and T. Miyajima, Microelectron. Eng. 2, 129 (1984).
- <sup>24</sup>S.-H. Bae, H. Kum, W. Kong, Y. Kim, C. Choi, B. Lee, P. Lin, Y. Park, and J. Kim, Nat. Mater. 18, 550 (2019).
- 25 Z. Rao, Y. Lu, Z. Li, K. Sim, Z. Ma, J. Xiao, and C. Yu, Nat. Electron. 4, 513 (2021).
- <sup>26</sup>M. S. Kim, G. J. Lee, C. Choi, M. S. Kim, M. Lee, S. Liu, K. W. Cho, H. M. Kim, H. Cho, M. K. Choi, N. Lu, Y. M. Song, and D. H. Kim, Nat. Electron. 3, 546 (2020).
- <sup>27</sup>Z. Zhang, Z. Tian, Y. Mei, and Z. Di, Mater. Sci. Eng. R Rep. 145, 100621 (2021).
- <sup>28</sup>M. Konagai, M. Sugimoto, and K. Takahashi, J. Cryst. Growth 45, 277 (1978).
- 29 S. Kim, J. H. Son, S. H. Lee, B. K. You, K. Park, H. K. Lee, M. Byun, and K. J. Lee, Adv. Mater. 26, 7480 (2014).
- <sup>30</sup>S. J. Kim, H. E. Lee, H. Choi, Y. Kim, J. H. We, J. S. Shin, K. J. Lee, and B. J. Cho, ACS Nano 10, 10851 (2016).
- <sup>31</sup>S. H. Lee, S. Y. Park, and K. J. Lee, *Biosensing and Nanomedicine V* (SPIE, 2012), pp. 150–155.
- <sup>32</sup>A. Rajan, D. J. Rogers, C. Ton-That, L. Zhu, M. R. Phillips, S. Sundaram, S. Gautier, T. Moudakir, Y. El-Gmili, and A. Ougazzaden, J. Phys. D: Appl. Phys. 49(31), 315105 (2016).
- <sup>33</sup>J. He, J. Zhang, S. Qian, X. Chen, J. Qian, X. Hou, J. Mu, W. Geng, J. Cho, and X. Chou, J. Alloys Compd. 807, 151696 (2019).
- <sup>34</sup>E. Yablonovitch, T. Gmitter, J. P. Harbison, and R. Bhat, Appl. Phys. Lett. 51, 2222 (1987).
- 35 E. Gao, S.-Z. Lin, Z. Qin, M. J. Buehler, X.-Q. Feng, and Z. Xu, J. Mech. Phys. Solids 115, 248–262 (2018).
- <sup>36</sup>Y. Huang, Y.-H. Pan, R. Yang, L.-H. Bao, L. Meng, H.-L. Luo, Y.-Q. Cai, G.-D. Liu, W.-J. Zhao, and Z. Zhou, Nat. Commun. 11, 2453 (2020).
- 37D. Du, S. Manzo, C. Zhang, V. Saraswat, K. T. Genser, K. M. Rabe, P. M. Voyles, M. S. Arnold, and J. K. Kawasaki, Nat. Commun. 12, 2494 (2021).
- <sup>38</sup>J. Jeong, Q. Wang, J. Cha, D. K. Jin, D. H. Shin, S. Kwon, B. K. Kang, J. H. Jang, W. S. Yang, and Y. S. Choi, Sci. Adv. 6(23), eaaz5180 (2020).
- <sup>39</sup>M. M. R. Evans, J. C. Glueckstein, and J. Nogami, *Phys. Rev. B* **53**, 4000 (1996).
- <sup>40</sup>H. Heo, J. H. Sung, J. Ahn, F. Ghahari, T. Taniguchi, K. Watanabe, P. Kim, and M. Jo, Adv. Electron. Mater. 3, 1600375 (2017).
- <sup>41</sup>T. Ayari, S. Sundaram, X. Li, Y. El Gmili, P. L. Voss, J. P. Salvestrini, and A. Ougazzaden, Appl. Phys. Lett. **108**, 171106 (2016).
- <sup>42</sup>C. R. A. Catlow and A. M. Stoneham, J. Phys. C: Solid State Phys. **16**, 4321 (1983)
- 43H. Gottschalk, G. Patzer, and H. Alexander, Phys. Status Solidi A 45, 207 (1978)
- <sup>44</sup>N. E. Christensen, S. Satpathy, and Z. Pawlowska, Phys. Rev. B 36, 1032 (1987)
- 45W. Gordy and W. J. O. Thomas, J. Chem. Phys. 24, 439 (1956).
- 46 J. C. Phillips, Rev. Mod. Phys. 42, 317 (1970).
- <sup>47</sup>K. Badokas, A. Kadys, J. Mickevičius, I. Ignatjev, M. Skapas, S. Stanionytė, E. Radiunas, G. Juška, and T. Malinauskas, J. Phys. D: Appl. Phys. 54, 205103 (2021).
- <sup>48</sup>J. Jeong, D. K. Jin, J. Cha, B. K. Kang, Q. Wang, J. Choi, S. W. Lee, V. Y. Mikhailovskii, V. Neplokh, and N. Amador-Mendez, ACS Appl. Nano Mater. 3(9), 8920–8930 (2020).
- 49 J. Yuan, J.-Q. Dai, and C. Ke, Comput. Mater. Sci. 200, 110811 (2021).
- <sup>50</sup>G. Migliato Marega, Z. Wang, M. Paliy, G. Giusi, S. Strangio, F. Castiglione, C. Callegari, M. Tripathi, A. Radenovic, and G. Iannaccone, ACS Nano 16(3), 3684–3694 (2022).
- <sup>51</sup>J. Lin, X. Chen, X. Duan, Z. Yu, W. Niu, M. Zhang, C. Liu, G. Li, Y. Liu, and X. Liu, Adv. Sci. 9(8), 2104439 (2022).
- A. Hwang, M. Park, Y. Park, Y. Shim, S. Youn, C.-H. Lee, H. B. Jeong, H. Y. Jeong, J. Chang, and K. Lee, Sci. Adv. 7(51), eabj2521 (2021).
- 53 Z. Yan, G. Liu, J. M. Khan, and A. A. Balandin, Nat. Commun. 3, 827 (2012).

- <sup>54</sup>W. Bao, Z. Wang, and G. Chen, Int. J. Heat Mass Transfer 173, 121266 (2021).
- <sup>55</sup>V. S. Volcheck and V. R. Stempitsky, J. Phys. Conf. Ser. **917**, 082015 (2017).
- <sup>56</sup>C. M. Leung, J. Li, D. Viehland, and X. Zhuang, J. Phys. D: Appl. Phys. 51, 263002 (2018).
- <sup>57</sup>U. Bauer, M. Przybylski, J. Kirschner, and G. S. D. Beach, Nano Lett. 12, 1437 (2012).
- <sup>58</sup> A. Beck, J. G. Bednorz, C. Gerber, C. Rossel, and D. Widmer, Appl. Phys. Lett. 77, 139 (2000).
- 59 Y. Wang, J. Hu, Y. Lin, and C.-W. Nan, NPG Asia Mater. 2, 61 (2010).
- <sup>60</sup>J. Hoffman, X. Pan, J. W. Reiner, F. J. Walker, J. P. Han, C. H. Ahn, and T. P. Ma, Adv. Mater. 22, 2957 (2010).
- <sup>61</sup>Y. Tokura, S. Seki, and N. Nagaosa, Rep. Prog. Phys. 77, 076501 (2014).
- 62 A. P. Pyatakov and A. K. Zvezdin, Phys.-Usp. 55, 557 (2012).
- 63 R. Ramesh and N. A. Spaldin, Nat. Mater. 6, 21 (2007).
- 64N. A. Spaldin and R. Ramesh, Nat. Mater. 18, 203 (2019).
- 65P. Zubko, S. Gariglio, M. Gabay, P. Ghosez, and J.-M. Triscone, Annu. Rev. Condens. Matter Phys. 2, 141 (2011).
- <sup>66</sup>R. A. McKee, F. J. Walker, and M. F. Chisholm, Phys. Rev. Lett. **81**, 3014 (1998).
- 67Y. H. Chu, npj Quantum Mater. 2, 67 (2017).
- <sup>68</sup>F. Griggio, S. Jesse, A. Kumar, O. Ovchinnikov, H. Kim, T. N. Jackson, D. Damjanovic, S. V. Kalinin, and S. Trolier-McKinstry, Phys. Rev. Lett. **108**, 157604 (2012).
- <sup>69</sup>R. N. Torah, S. P. Beeby, and N. M. White, J. Phys. D: Appl. Phys. 37, 1074 (2004)
- <sup>70</sup>A. Almusallam, K. Yang, D. Zhu, R. N. Torah, A. Komolafe, J. Tudor, and S. P. Beeby, Smart Mater. Struct. 24, 115030 (2015).
- 71 B. Fu, R. Lu, K. Gao, Y. Yang, and Y. Wang, Europhys. Lett. 112, 27002 (2015).
  72 H. Lee, N. Campbell, J. Lee, T. J. Asel, T. R. Paudel, H. Zhou, J. W. Lee, B. Noesges, J. Seo, B. Park, L. J. Brillson, S. H. Oh, E. Y. Tsymbal, M. S. Rzchowski, and C. B. Eom, Nat. Mater. 17, 231 (2018).
- <sup>73</sup>M. Boota, E. P. Houwman, M. D. Nguyen, G. Lanzara, and G. Rijnders, AIP Adv. 6, 055303 (2016).
- <sup>74</sup>G. Tian, F. Zhang, J. Yao, H. Fan, P. Li, Z. Li, X. Song, X. Zhang, M. Qin, M. Zeng, Z. Zhang, J. Yao, X. Gao, and J. Liu, ACS Nano 10, 1025 (2016).
- 75J. Zhang, X. Ke, G. Gou, J. Seidel, B. Xiang, P. Yu, W.-I. Liang, A. M. Minor, Y. Chu, G. Van Tendeloo, X. Ren, and R. Ramesh, Nat. Commun. 4, 2768
- (2013).

  <sup>76</sup>V. Nagarajan, A. Roytburd, A. Stanishevsky, S. Prasertchoung, T. Zhao, L. Chen, J. Melngailis, O. Auciello, and R. Ramesh, Nat. Mater. 2, 43 (2003).
- <sup>77</sup>D. M. Paskiewicz, R. Sichel-Tissot, E. Karapetrova, L. Stan, and D. D. Fong, Nano Lett. 16, 534 (2016).
- 78S. R. Bakaul, C. R. Serrao, M. Lee, C. W. Yeung, A. Sarker, S.-L. Hsu, A. K. Yadav, L. Dedon, L. You, A. I. Khan, J. D. Clarkson, C. Hu, R. Ramesh, and S. Salahuddin, Nat. Commun. 7, 10547 (2016).
- <sup>79</sup>D. Lu, D. J. Baek, S. S. Hong, L. F. Kourkoutis, Y. Hikita, and H. Y. Hwang, Nat. Mater. 15, 1255 (2016).
- 80 H. Coy-Diaz, R. Addou, and M. Batzill, J. Phys. Chem. C 117, 21006 (2013).
- <sup>81</sup>P. R. Willmott, R. Herger, C. M. Schlepütz, D. Martoccia, and B. D. Patterson, Phys. Rev. Lett. 96, 176102 (2006).
- <sup>82</sup>D. Ji, S. Cai, T. Paudel, H. Sun, C. Zhang, L. Han, Y. Wei, Y. Zang, M. Gu, Y. Zhang, W. Gao, H. Huyan, W. Guo, D. Wu, Z. Gu, E. Tsymbal, P. Wang, Y. Nie, and X. Pan, Nature 570, 87 (2019).
- <sup>83</sup>N. M. Aimon, D. Hun Kim, H. Kyoon Choi, and C. A. Ross, Appl. Phys. Lett. 100, 092901 (2012).
- <sup>84</sup>F. Heyroth, C. Hauser, P. Trempler, P. Geyer, F. Syrowatka, R. Dreyer, S. G. Ebbinghaus, G. Woltersdorf, and G. Schmidt, Phys. Rev. Appl. **12**, 54031 (2019)
- 85 J. Kim and Y.-H. Xie, Appl. Phys. Lett. 89, 152117 (2006).
- 86S. Leontsev, P. J. Shah, H. S. Kum, J. L. McChesney, F. M. Rodolakis, M. van Veenendaal, M. Velez, R. Rao, D. Haskel, and J. Kim, J. Magn. Magn. Mater. 556, 169440 (2022).

- <sup>87</sup>T. Löher, Y. Tomm, C. Pettenkofer, and W. Jaegermann, Appl. Phys. Lett. 65, 555 (1994).
- 88 A. Koma, J. Cryst. Growth 201-202, 236 (1999).
- 89 A. Koma, Thin Solid Films 216, 72 (1992).
- 90 A. Koma, K. Ueno, and K. Saiki, J. Cryst. Growth 111, 1029 (1991).
- 91 A. Koma and K. Yoshimura, Surf. Sci. 174, 556 (1986).
- 92S. Steinberg *et al.*, Science 260(5108), 656–659 (1993).
- 93 Y. Bitla and Y.-H. Chu, FlatChem. 3, 26 (2017).
- <sup>94</sup>M. I. B. Utama, F. J. Belarre, C. Magen, B. Peng, J. Arbiol, and Q. Xiong, Nano Lett. 12, 2146 (2012).
- <sup>95</sup>C.-H. Ma, J.-C. Lin, H.-J. Liu, T. H. Do, Y.-M. Zhu, T. D. Ha, Q. Zhan, J.-Y. Juang, Q. He, E. Arenholz, P.-W. Chiu, and Y.-H. Chu, Appl. Phys. Lett. 108, 253104 (2016).
- <sup>96</sup>Y. He, H. Dong, Q. Meng, L. Jiang, W. Shao, L. He, and W. Hu, Adv. Mater. 23, 5502 (2011).
- <sup>97</sup>Y. Bitla, C. Chen, H. C. Lee, T. H. Do, C. H. Ma, L. Van Qui, C. W. Huang, W. W. Wu, L. Chang, P. W. Chiu, and Y. H. Chu, ACS Appl. Mater. Interfaces 8, 32401 (2016).
- 98S. Yang, S. Han, R. Li, and K. Sheng, in 2018 IEEE 30th International Symposium on Power Semiconductor Devices and ICs (ISPSD) (IEEE, 2018), pp. 272–275.
- pp. 272–275.

  99 Z. Z. Bandić, P. M. Bridger, E. C. Piquette, T. C. McGill, R. P. Vaudo, V. M. Phanse, and J. M. Redwing, Appl. Phys. Lett. 74, 1266 (1999).
- 100 J. Jeong, D. K. Jin, J. Choi, J. Jang, B. K. Kang, Q. Wang, W. Il Park, M. S. Jeong, B.-S. Bae, and W. S. Yang, Nano Energy 86, 106075 (2021).
- 101 C. X. Xue, Y. C. Chiu, T. W. Liu, T. Y. Huang, J. S. Liu, T. W. Chang, H. Y. Kao, J. H. Wang, S. Y. Wei, C. Y. Lee, S. P. Huang, J. M. Hung, S. H. Teng, W. C. Wei, Y. R. Chen, T. H. Hsu, Y. K. Chen, Y. C. Lo, T. H. Wen, C. C. Lo, R. S. Liu, C. C. Hsieh, K. T. Tang, M. S. Ho, C. Y. Su, C. C. Chou, Y. Der Chih, and M. F. Chang, Nat. Electron. 4, 81 (2021).
- 102 Z. Chen, Z. Liu, T. Wei, S. Yang, Z. Dou, Y. Wang, H. Ci, H. Chang, Y. Qi, and J. Yan, Adv. Mater. 31, 1807345 (2019).
- 103S. W. Bedell, D. Shahrjerdi, B. Hekmatshoar, K. Fogel, P. A. Lauro, J. A. Ott, N. Sosa, and D. Sadana, IEEE J. Photovoltaic 2, 141 (2012).
- 104A. Lamoureux, K. Lee, M. Shlian, S. R. Forrest, and M. Shtein, Nat. Commun. 6, 8092 (2015).
- 105 T. Ayari, S. Sundaram, X. Li, S. Alam, C. Bishop, W. El Huni, M. B. Jordan, Y. Halfaya, S. Gautier, and P. L. Voss, ACS Photonics 5(8), 3003–3008 (2018).
- 106C.-R. Huang, H.-C. Chiu, C.-H. Liu, H.-C. Wang, H.-L. Kao, C.-T. Chen, and K.-J. Chang, Membranes (Basel) 11, 848 (2021).
- 107F. Ejeckam, D. Francis, F. Faili, J. Dodson, D. J. Twitchen, B. Bolliger, and D. Babic, in Fourteenth Intersociety Conference on Thermal and Thermomechanical Phenomena in Electronic Systems (ITherm) (IEEE, 2014), pp. 1206–1209.
- 108°C. Guo, G. Dong, Z. Zhou, M. Liu, H. Huang, J. Hong, and X. Wang, Appl. Phys. Lett. 116, 152903 (2020).
- 109 G. Zhong, F. An, K. Qu, Y. Dong, Z. Yang, L. Dai, S. Xie, R. Huang, Z. Luo, and J. Li, Small 18, 2104213 (2022).
- <sup>110</sup>A. Brewer, K. H. Cho, W. Saenrang, S. H. Baek, J. C. Frederick, and C. B. Eom, J. Vac. Sci. Technol. A 35, 060607 (2017).
- 1111X. Gao, B. J. Rodriguez, L. Liu, B. Birajdar, D. Pantel, M. Ziese, M. Alexe, and D. Hesse, ACS Nano 4, 1099 (2010).
- <sup>112</sup>V.-Q. Le, T.-H. Do, J. R. D. Retamal, P.-W. Shao, Y.-H. Lai, W.-W. Wu, J.-H. He, Y.-L. Chueh, and Y.-H. Chu, Nano Energy 56, 322 (2019).

- <sup>113</sup>J. Jiang, Y. Bitla, C.-W. Huang, T. H. Do, H.-J. Liu, Y.-H. Hsieh, C.-H. Ma, C.-Y. Jang, Y.-H. Lai, and P.-W. Chiu, Sci. Adv. 3(6), e1700121 (2017).
- 114H.-J. Liu, C.-K. Wang, D. Su, T. Amrillah, Y.-H. Hsieh, K.-H. Wu, Y.-C. Chen, J.-Y. Juang, L. M. Eng, S.-U. Jen, and Y.-H. Chu, ACS Appl. Mater. Interfaces 9, 7297 (2017).
- <sup>115</sup>C. Mattevi, H. Kim, and M. Chhowalla, J. Mater. Chem. **21**, 3324 (2011).
- <sup>116</sup>B. Zhang, W. H. Lee, R. Piner, I. Kholmanov, Y. Wu, H. Li, H. Ji, and R. S. Ruoff, ACS Nano 6, 2471 (2012).
- 117] J. Shim, S.-H. Bae, W. Kong, D. Lee, K. Qiao, D. Nezich, Y. J. Park, R. Zhao, S. Sundaram, X. Li, H. Yeon, C. Choi, H. Kum, R. Yue, G. Zhou, Y. Ou, K. Lee, J. Moodera, X. Zhao, J.-H. Ahn, C. Hinkle, A. Ougazzaden, and J. Kim, Science 362(6415), 665–670 (2018).
- <sup>118</sup>V. Panchal, Y. Yang, G. Cheng, J. Hu, M. Kruskopf, C.-I. Liu, A. F. Rigosi, C. Melios, A. R. Hight Walker, D. B. Newell, O. Kazakova, and R. E. Elmquist, Commun. Phys. 1, 83 (2018).
- 119 J. Y. Yang, M. J. Yeom, J. Lee, K. Lee, C. Park, J. Heo, and G. Yoo, Adv. Electron. Mater. 8, 2101406 (2022).
- <sup>120</sup>J. Wu, H.-Y. Chen, N. Yang, J. Cao, X. Yan, F. Liu, Q. Sun, X. Ling, J. Guo, and H. Wang, Nat. Electron. 3(8), 466–472 (2020).
- <sup>121</sup>A. J. Molina-mendoza and T. Mueller, Nature **579**, 62–66 (2020).
- 122J. Jeon, S. K. Jang, S. M. Jeon, G. Yoo, Y. H. Jang, J.-H. Park, and S. Lee, Nanoscale 7, 1688 (2015).
- <sup>123</sup>D. J. Hynek, R. M. Singhania, S. Xu, B. Davis, L. Wang, M. Yarali, J. v Pondick, J. M. Woods, N. C. Strandwitz, and J. J. Cha, ACS Nano 15(1), 410–418 (2020).
- 124<sub>J.</sub>-H. Lee, E. K. Lee, W.-J. Joo, Y. Jang, B.-S. Kim, J. Y. Lim, S.-H. Choi, S. J. Ahn, J. R. Ahn, and M.-H. Park, Science 344(6181), 286–289 (2014).
- S. J. Ahn, J. R. Ahn, and M.-H. Park, Science 344(6181), 286–289 (2014).

  125 A. Chaves, J. G. Azadani, H. Alsalman, D. R. da Costa, R. Frisenda, A. J. Chaves, S. H. Song, Y. D. Kim, D. He, and J. Zhou, npj 2D Mater. Appl. 4, 20 (2020)
- 126D. Geng and H. Y. Yang, Adv. Mater. 30, 1800865 (2018).
- 127 Z. Wu, Y. Lyu, Y. Zhang, R. Ding, B. Zheng, Z. Yang, S. P. Lau, X. H. Chen, and J. Hao, Nat. Mater. 20, 1203 (2021).
- 128 H. Ryu, K. Xu, D. Li, X. Hong, and W. Zhu, Appl. Phys. Lett. 117, 080503 (2020).
- 129H. Chang, Z. Chen, W. Li, J. Yan, R. Hou, S. Yang, Z. Liu, G. Yuan, J. Wang, and J. Li, Appl. Phys. Lett. 114, 091107 (2019).
- 130 S. Yang, P. Luo, F. Wang, T. Liu, Y. Zhao, Y. Ma, H. Li, and T. Zhai, Small 18, 2105211 (2021).
- <sup>131</sup>D. Wang, Y. Lu, J. Meng, X. Zhang, Z. Yin, M. Gao, Y. Wang, L. Cheng, J. You, and J. Zhang, Nanoscale 11, 9310 (2019).
- 132S. Das, A. Sebastian, E. Pop, C. J. McClellan, A. D. Franklin, T. Grasser, T. Knobloch, Y. Illarionov, A. V. Penumatcha, and J. Appenzeller, Nat. Electron. 4(11), 786–799 (2021).
- 133 S. Kumar, R. S. Williams, and Z. Wang, Nature 585, 518 (2020).
- 134Y. Liu, IEEE Trans. Adv. Packag. 25, 43 (2002).
- 135 J. Ge, X. Wang, M. Drack, O. Volkov, M. Liang, G. S. Cañón Bermúdez, R. Illing, C. Wang, S. Zhou, and J. Fassbender, Nat. Commun. 10, 4405 (2019).
- <sup>136</sup>H. Yeon, H. Lee, Y. Kim, D. Lee, Y. Lee, J. S. Lee, J. Shin, C. Choi, J. H. Kang, J. M. Suh, H. Kim, H. S. Kum, J. Lee, D. Kim, K. Ko, B. S. Ma, P. Lin, S. Han, S. Kim, S. H. Bae, T. S. Kim, M. C. Park, Y. C. Joo, E. Kim, J. Han, and J. Kim, Sci. Adv. 7, eabg8459 (2021).